JOURNAL OF SPACECRAFT AND ROCKETS
Vol. 46, No. 5, September–October 2009

Capabilities of Furlable Solar Sails for Asteroid Proximity Operations

Trevor Williams*
University of Cincinnati, Cincinnati, Ohio 45221
and
Matthew Abate†
Orbital Sciences Corporation, Dulles, Virginia 20166

DOI: 10.2514/1.30355

Missions have been proposed in which a spacecraft equipped with a large furlable solar sail transfers to a main-belt asteroid using the fully deployed sail for propulsion and then performs an inspection mission at the asteroid with the sail fully stowed. This paper examines ways in which the partially deployed sail could instead be used to maneuver the spacecraft while in the vicinity of the asteroid, with the goal of improving the science observations that could be made. Methods are presented for quantifying the performance that can be obtained by taking advantage of the freedom to select the active sail area for two types of hovering problems: one in which the spacecraft is to maintain a fixed position in the rotating sun–asteroid frame and the other in which it is to maintain a fixed position relative to a landmark on the rotating asteroid surface. In both of these problems, the ability to adjust the active sail area greatly expands the range of locations at which the spacecraft can satisfy the specified hover conditions.

Nomenclature

A	=	solar sail area, m^2
$A(r)$, $B(r)$, $C(r)$	=	acceleration component scalings in the heliostationary flight problem, $1/s^2$
a, e, i, Ω, ω, M_o	=	classical elements of solar sail orbit about an asteroid, various units
$\mathbf{a}_g$, $\mathbf{a}_{\text{des}}$, $\mathbf{a}_{\text{sail}}$	=	gravitational, desired, and solar sail acceleration vectors, m/s^2
$a_{\max}$	=	maximum achievable solar sail acceleration, m/s^2
a_R, a_S, a_W	=	solar sail acceleration components expressed in the *RSW* orbital frame, m/s^2
a_{sail}	=	magnitude of solar radiation pressure acceleration on the sail, m/s^2
m	=	solar sail spacecraft mass, kg
n	=	solar sail orbit mean motion, rad/s
p	=	solar radiation pressure, N/m^2
p_E	=	solar radiation pressure in the vicinity of the Earth, 4.56×10^{-6} N/m^2
q_{bc}	=	variation-of-parameters influence coefficient for variable b from acceleration component c, various units
R_{AU}	=	distance of the asteroid from the sun, astronomical units
r_{ast}	=	asteroid radius, m
r_L	=	asteroid L_1/L_2 libration point radius, m
r_{pole}	=	radius lower limit on the polar segment of the heliostationary flight solution, m
r_{sync}	=	asteroid synchronous orbit, or resonance, radius, m
r_1, r_2	=	lower and upper limits on solution radii for the heliostationary flight problem, m
$\hat{\mathbf{s}}$	=	unit vector directed from the sun to the asteroid, dimensionless
u	=	solar sail orbit argument of latitude, rad
x, y, z	=	relative orbital position components expressed in the *RSW* orbital frame, m
x_1, x_2	=	modified asteroid libration point radii for the solar sail, m
α	=	angle between sail normal and sun line (i.e., sail cone angle), rad
γ	=	solar sail viewing angle of the illuminated asteroid hemisphere, rad
δ_1, δ_2	=	measures of difficulty for the body-fixed hovering problem, m^3/s^2
λ	=	latitude of sail target point on the asteroid, rad
θ	=	asteroid longitude, rad
η	=	solar sail efficiency factor, dimensionless
μ_{ast}	=	gravitational parameter of the asteroid, m^3/s^2
ν	=	solar sail orbit mean true anomaly, rad
φ	=	solar latitude, perpendicular angle between the sun line and equatorial plane of the asteroid, rad
ψ	=	solar sail clock angle, rad
ω_{ast}	=	rotation rate of the asteroid, rad/s

Introduction

THE NASA Autonomous Nano-Technology Swarm (ANTS) concept [1,2] is based on the use of swarms of very small spacecraft (nominally 1 kg picosatellites) equipped with large segmented solar sails [3] (nominally with a fully exposed area of 100 m^2). One key mission that has been proposed for ANTS is the Prospecting Asteroid Mission. The high area-to-mass ratio of these designs leads to flight times from Earth to the main belt [4] on the order of 2.5 years, with these trajectories well defined from previous studies. However, how best to exploit the solar force that acts on the sail once the spacecraft is operating in the vicinity of an asteroid is not so clear. This question served as motivation for the work that is described in this paper.

Three possible goals will be considered, the first being general orbital adjustments. These would occur, for instance, if the spacecraft were to be transferred from an equatorial to a polar orbit or if the orbit were to be circularized. It is shown that a spacecraft such as ANTS would be capable of very rapid orbit changes of this type.

Received 8 February 2007; revision received 25 February 2008; accepted for publication 28 March 2008.

*Professor, Department of Aerospace Engineering; currently Aerospace Engineer, Navigation and Mission Design Branch, NASA Goddard Space Flight Center, Greenbelt, MD 20771. Associate Fellow AIAA.

†Guidance, Navigation, and Control Engineer, Guidance, Navigation, and Control Design and Analysis Group, 21839 Atlantic Boulevard.

The second maneuvering goal is to cause the spacecraft to maintain a fixed position in the rotating sun–asteroid frame: this is termed *heliostationary flight* in this paper. For instance, hovering over the subsolar point would be of great interest for remote sensing. In the absence of some form of thrusting, the only locations at which heliostationary flight is possible are the sun–asteroid libration points; the object of this work is to determine how these points generalize when a solar sail is added to the spacecraft. It is shown that for a spacecraft equipped with a fixed-area solar sail, the libration points generalize to two-dimensional hover surfaces. For a spacecraft such as ANTS that is equipped with a furlable solar sail, these surfaces generalize still further to hover regions, thus providing significantly increased freedom for the mission designer.

The third maneuvering goal is to maintain a fixed position relative to the surface of the rotating asteroid. In the terminology of [5–8], this is the *body-fixed hovering* problem; it could also be referred to as *asterostationary flight*, by analogy with heliostationary flight. Such a trajectory would allow a specific crater or other surface feature on the asteroid to be studied for extended periods of time or could prove useful as a prelude to landing operations. The solar sail in this case can be thought of as being used to generalize the synchronous orbit (or *resonance radius* [7]) points about the asteroid. In analogous fashion to the results obtained for the heliostationary flight problem, the synchronous points are shown to generalize to two-dimensional surfaces for a spacecraft that is equipped with a fixed-area solar sail and to entire regions for a spacecraft with a furlable sail. Furthermore, the geometry of these regions is shown to depend greatly upon the orientation of the sun line relative to the asteroid spin axis. The results presented complement those for hovering flight near an asteroid that were derived in [5–7] for spacecraft equipped with a continuous-thrust propulsion system, as opposed to a solar sail, as well as those for a fixed-area sail presented in [8], and the order of magnitude quantities developed in [9] for proximity operations at small bodies.

Solar Radiation Pressure Formulation

The total acceleration magnitude that is exerted by solar radiation pressure (SRP) on a sail-equipped spacecraft with area-to-mass ratio A/m can be written [3] as

$$a_{\text{sail}} = 2\eta p(A/m)\cos^2\alpha \tag{1}$$

where the sail efficiency factor η will be taken as 0.85 here to reflect, to first order, the variation of the true sail from an ideal (perfectly flat and specularly reflective) one. The inverse square law nature of solar radiation implies that the radiation pressure in the vicinity of an asteroid is given as $p = p_E/R_{\text{AU}}^2$. For an ideal sail, this acceleration vector is directed along the sail normal lying in the down-sun hemisphere; for a real sail, it will lie along approximately this direction, but with increasing deviation in the regime in which α approaches 90 deg.

Consider a case that is intended to be representative of a main-belt asteroid: asteroid diameter 5 km, density 2.5×10^3 kg/m^3, and distance 2.7 AU (astronomical units) from the sun, being orbited by an ANTS spacecraft with a fully unfurled sail, giving an A/m value of 100 m^2/kg. It can be shown that when broadside to the sun, the sail produces an acceleration that is equal to the gravitational acceleration that the asteroid exerts on the spacecraft when at a radial position of 10.1 km. It is for this reason that it is hoped that solar sails can be powerful tools for flight in the proximity of asteroids. The remainder of the paper will now examine the details of several specific applications of this approach.

General Orbital Maneuvers

The first problem will be that of executing large arbitrary changes in the orbit that the sail-equipped spacecraft follows about the asteroid. The Gaussian variation-of-parameters (VOP) orbital perturbation equations [10] are very useful for such studies, allowing the computation of the continuous variations in the orbital elements that are caused by the continuous solar sail acceleration.

The VOP equations are expressed here in terms of the local *RSW* frame [10]: the *R* vector is directed along the outward radius, the *S* vector is along the forward tangential direction (this coincides with the velocity vector in the circular orbit case), and *W* is along the orbit normal (angular momentum vector). Expressing the solar sail acceleration in terms of its components a_R, a_S, and a_W in the *RSW* frame, the resulting instantaneous rates of change of the orbital elements (semimajor axis a, eccentricity e, inclination i, longitude of ascending node Ω, argument of perigee ω, and mean anomaly at epoch M_o) are as shown next.

Semimajor axis:

$$\dot{a} = q_{aR}a_R + q_{aS}a_S + q_{aW}a_W \tag{2}$$

where

$$q_{aR}(\nu) = \frac{2}{n}\frac{e}{\sqrt{1-e^2}}\sin\nu, \qquad q_{aS}(\nu) = \frac{2}{n}\frac{(1+e\cos\nu)}{\sqrt{1-e^2}}$$
$$q_{aW}(\nu) = 0 \tag{3}$$

In these expressions, ν is the true anomaly of the satellite and n is the mean motion, or mean angular rate, of the orbit: $n = \sqrt{\mu/a^3}$, where μ is the gravitational parameter of the asteroid.

Eccentricity:

$$\dot{e} = q_{eR}a_R + q_{eS}a_S + q_{eW}a_W \tag{4}$$

with

$$q_{eR}(\nu) = \frac{\sqrt{1-e^2}}{na}\sin\nu$$
$$q_{eS}(\nu) = \frac{\sqrt{1-e^2}}{na}\frac{2\cos\nu + e(1+\cos^2\nu)}{1+e\cos\nu}, \quad q_{eW}(\nu) = 0 \tag{5}$$

Inclination:

$$\dot{i} = q_{iR}a_R + q_{iS}a_S + q_{iW}a_W \tag{6}$$

with

$$q_{iR}(\nu) = q_{iS}(\nu) = 0, \qquad q_{iW}(\nu) = \frac{\sqrt{1-e^2}}{na}\frac{\cos u}{(1+e\cos\nu)} \tag{7}$$

In this expression, $u = \omega + \nu$ is the argument of latitude (i.e., the angle from the ascending node of the orbit to the satellite, measured in the orbital plane) in the direction of motion.

Longitude of ascending node (LAN):

$$\dot{\Omega} = q_{\Omega R}a_R + q_{\Omega S}a_S + q_{\Omega W}a_W \tag{8}$$

with

$$q_{\Omega R}(\nu) = q_{\Omega S}(\nu) = 0, \quad q_{\Omega W}(\nu) = \frac{\sqrt{1-e^2}}{na}\frac{\sin u}{\sin i(1+e\cos\nu)} \tag{9}$$

Argument of perigee:

$$\dot{\omega} = q_{\omega R}a_R + q_{\omega S}a_S + q_{\omega W}a_W \tag{10}$$

with

$$q_{\omega R}(\nu) = -\frac{\sqrt{1-e^2}}{nae}\cos\nu$$
$$q_{\omega S}(\nu) = \frac{\sqrt{1-e^2}}{nae}\frac{2+e\cos\nu}{1+e\cos\nu}\sin\nu$$
$$q_{\omega W}(\nu) = -\frac{\sqrt{1-e^2}}{na}\frac{\cot i\sin u}{1+e\cos\nu} \tag{11}$$

Mean anomaly at epoch:

$$\dot{M}_o = q_{M_oR}a_R + q_{M_oS}a_S - t\dot{n} \tag{12}$$

with

$$q_{M_o R}(\nu) = -\frac{1-e^2}{nae}\frac{e(2-\cos^2\nu)-\cos\nu}{1+e\cos\nu}$$
$$q_{M_o S}(\nu) = -\frac{1-e^2}{nae}\frac{2+e\cos\nu}{1+e\cos\nu}\sin\nu \tag{13}$$

Numerical results will now be given for the specific case of an ANTS spacecraft with a fully deployed sail (A/m of 100 m^2/kg) orbiting a hypothetical spherically symmetric body with the same gravitational parameter (4.46×10^5 m^3/s^2) as asteroid 433 Eros, in an orbit with semimajor axis (1.458 AU) equal to that of Eros. The corresponding solar radiation pressure is 2.12×10^{-6} N/m^2. Five initial spacecraft orbits are considered, with semimajor axes ranging from 17 to 65 km; the corresponding orbital periods vary from 5.8 to 43.3 h. In all cases, the orbit is initially near-circular (eccentricity 0.001) with an inclination of 30 deg. Figure 1 shows the changes that can be produced in LAN by the ANTS solar sail over the course of two spacecraft orbits. It can be seen that very large changes (exceeding 360 deg for the highest orbit) can be made to Ω in this short interval, despite the fact that the sail must be "turned off" periodically by putting it edge-on to the sun to avoid ever-reducing Ω. (The timing of these switches depends on the sign of $\sin u$ [see the second equation in Eq. (9)].) Figure 2 gives corresponding plots for the achievable shifts in inclination from the initial value of 30 deg; it can be seen that the solar sail can again produce large changes in this parameter very quickly.

These large, rapid changes in the orbital elements confirm that the acceleration that is produced by a large solar sail can indeed lead to significantly non-Keplerian flight about an asteroid. The remainder of the paper will now examine two specific types of desired non-Keplerian flight to determine the performance of the solar sail in these particular cases. Both scenarios have the spacecraft attempting to maintain a fixed position relative to some specific coordinate system: in the first, the coordinate system is fixed relative to the asteroid and sun; in the second, it is fixed relative to the rotating asteroid.

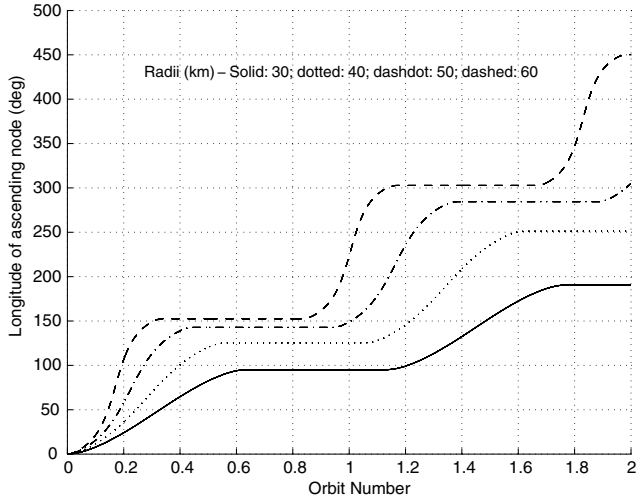

Fig. 1 Evolution of longitude of the ascending node with a solar sail.

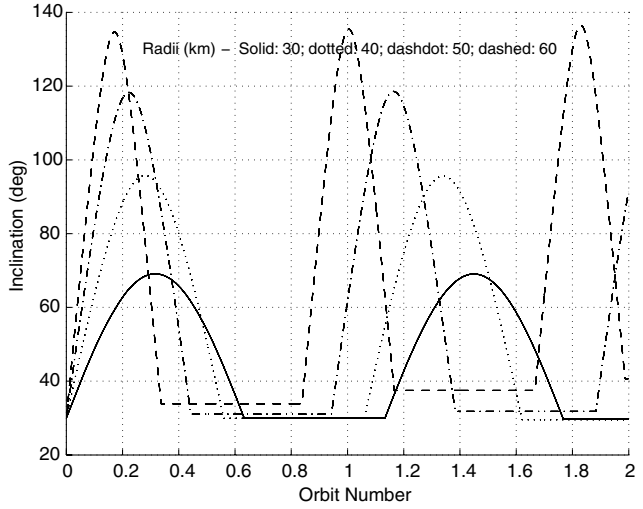

Fig. 2 Evolution of inclination with a solar sail.

Heliostationary Flight

The term *heliostationary flight* will be used here to signify motion in which the spacecraft maintains a fixed position relative to both the sun and asteroid, thus allowing prolonged viewing of the asteroid under constant lighting. Specifically, the spacecraft will be required to maintain a fixed position in the coordinate system that is centered on the asteroid and rotating to keep its $+x$ axis directed from the sun to the center of the asteroid, its $+y$ axis along the asteroid heliocentric velocity vector (if the orbit is circular), and its $+z$ axis along its orbit normal. In this coordinate system, the sun–asteroid libration points become fixed.

The equations of motion of the spacecraft around the asteroid are presented in this rotating frame. These are the linearized Hill or Clohessy–Wiltshire equations [10], with the addition of spherical asteroid gravity terms, as used in [6]. The following simplifying assumptions underlie these equations: the spacecraft remains in the neighborhood of the asteroid in heliocentric terms, allowing linearized heliocentric relative orbital motion equations to be used; no other perturbations in addition to solar radiation pressure are considered (e.g., Jovian effects, etc.); and the gravitational potential of the asteroid is spherically symmetric and its orbit is circular. The resulting equations of motion are

$$\ddot{x} = 2n\dot{y} - (\mu_{\text{ast}}/r^3)x + 3n^2x + a_x$$
$$\ddot{y} = -2n\dot{x} - (\mu_{\text{ast}}/r^3)y + a_y$$
$$\ddot{z} = -(\mu_{\text{ast}}/r^3)z - n^2z + a_z \tag{14}$$

In these equations, μ_{ast} is the gravitational parameter of the asteroid; $r = \sqrt{x^2+y^2+z^2}$ is the distance of the spacecraft from its center; n is its heliocentric mean motion, and a_x, a_y, and a_z are the components of nongravitational acceleration in the sun–asteroid coordinate frame.

If the only source of nongravitational force is generated by a solar sail, the acceleration components a_x, a_y, and a_z are quite constrained, thus also leading to tight constraints on the possible positions at which such a spacecraft can hover. This is quite different from the case studied in [5–8], in which the nongravitational force that is used to hold the spacecraft in its hovering location is produced by propulsive means and is thus unconstrained. For the solar sail case, if the solar sail has *cone angle* α (angle between the sail normal and the x axis, or sun vector) and *clock angle* ψ (angle between the y axis and the projection of the sail normal onto the y–z plane), then the resulting solar acceleration components are given as

$$a_x = a_{\text{sail}}\cos\alpha \tag{15a}$$

$$a_y = a_{\text{sail}}\sin\alpha\cos\psi \tag{15b}$$

$$a_z = a_{\text{sail}}\sin\alpha\sin\psi \tag{15c}$$

where a_{sail} is the total SRP acceleration acting on the sail, given by Eq. (1). A basic constraint on the solar acceleration vector is that it must always lie in the down-sun hemisphere. Equivalently, $a_x \geq 0$ always, as can be seen from Eq. (15a) and the fact that the cone angle α between the sun vector and the normal to the illuminated sail face can never exceed 90 deg.

If the spacecraft is to hover over the asteroid at position $(x \quad y \quad z)$, we must have $\ddot{x} = \ddot{y} = \ddot{z} = 0$ and $\dot{x} = \dot{y} = \dot{z} = 0$. Hence, from Eq. (14) we need

$$a_x = [(\mu_{\text{ast}}/r^3) - 3n^2]x \equiv A(r)x \tag{16a}$$

$$a_y = (\mu_{\text{ast}}/r^3)y \equiv B(r)y \tag{16b}$$

$$a_z = [(\mu_{\text{ast}}/r^3) + n^2]z \equiv C(r)z \tag{16c}$$

Note that the three scaling functions $A(r)$, $B(r)$, and $C(r)$ satisfy $C(r) > B(r) > A(r)$ for any radius r, with their relative differences increasing with increasing radius.

Because $a_x \geq 0$ always, Eq. (16a) implies that there are two regions in which any hovering solutions must lie:

1) Sunward (i.e., $x < 0$), we must have that $(\mu_{\text{ast}}/r^3) - 3n^2 \leq 0$: that is,

$$r^3 \geq (\mu_{\text{ast}}/3n^2) \tag{17}$$

2) Down-sun (i.e., $x > 0$), $(\mu_{\text{ast}}/r^3) - 3n^2 \geq 0$ must hold: that is,

$$r^3 \leq (\mu_{\text{ast}}/3n^2) \tag{18}$$

In other words, any sunward hover points must be quite far from the asteroid, at radii no lower than the L_1/L_2 *libration point radius*:

$$r_L \equiv \sqrt[3]{\mu_{\text{ast}}/3n^2} \tag{19}$$

As a result, any sunward hover points that are obtainable by means of a solar sail are almost certainly too far from the asteroid to be of practical interest. Down-sun hover points, by contrast, must all have ranges less than this limit. It is therefore possible that some of these may prove to be useful if unshadowed points can be found with good viewing of the illuminated portion of the asteroid.

Bounds on the locations of all possible solar sail hover points will now be examined in more detail. As a first step, consider hover points on the x axis, either sunward or antisun (i.e., points for which $y = z = 0$). From Eq. (16), we then clearly have $a_y = a_z = 0$, and so, from Eq. (15), $\alpha = 0$, and thus $a_x = a_{\max}$, where

$$a_{\max} = 2\eta p(A/m) \tag{20}$$

is the maximum solar acceleration that the sail can provide (when the solar sail is broadside to the sun). The x component of Eq. (14) then becomes, for a hover,

$$\ddot{x} = -(\mu_{\text{ast}}/r^3)x + 3n^2x + a_{\max} = 0$$

This equation takes two forms, depending on whether a sunward or down-sun position is considered.

1) Sunward, $x < 0$, and thus $x = -|x|$ and $r = |x|$; the hover equation becomes

$$(\mu_{\text{ast}}/|x|^2) - 3n^2|x| + a_{\max} = 0$$

or

$$3n^2|x|^3 - a_{\max}|x|^2 - \mu_{\text{ast}} = 0 \tag{21}$$

2) Down-sun, $x > 0$, and thus $r = x$, giving the hover equation

$$-(\mu_{\text{ast}}/x^2) + 3n^2x + a_{\max} = 0$$

or

$$3n^2x^3 + a_{\max}x^2 - \mu_{\text{ast}} = 0 \tag{22}$$

Thus, in the absence of a solar sail ($a_{\max} = 0$), these hover points are at equal distances from the center of the asteroid, at the sun–asteroid L_1 and L_2 libration points. As the sail area is increased, the sunward x-axis hover point moves (rapidly) farther out from the asteroid and the down-sun point moves closer in. A physical interpretation of this behavior is as follows. The libration points are those at which a satellite will have the same heliocentric angular rate as does the asteroid in its orbit. If acted upon solely by the sun, a body at the sunward L_1 point would orbit more rapidly than the asteroid. The gravitational acceleration of the asteroid serves to counteract a portion of that of the sun, thus making it appear that the body is orbiting a smaller virtual sun. The resulting orbital angular rate is therefore reduced, matching that of the asteroid. Likewise, a body at the down-sun L_2 libration point would, if acted upon only by the sun, have a heliocentric angular rate lower than that of the asteroid. The asteroid gravitational acceleration in this case, being sunward, reinforces that of the sun, thus making it appear that the body is orbiting a larger virtual sun. The resulting orbital angular rate is therefore increased, matching that of the asteroid. Adding a solar sail always increases the down-sun force on the satellite. In the case of the sunward hover point, this augments the asteroid gravitational acceleration, making the asteroid appear larger and thus shifting the hover point farther away from it. (This is the principle behind proposed GeoSail solar weather observatory mission [11], in which a solar sail would be used to shift a spacecraft to a halo orbit considerably sunward of the sun–Earth L_1 point, thus providing increased warning time of any incoming solar storms.) Conversely, the solar radiation acceleration at the antisun hover point partially cancels the gravitational acceleration of the asteroid, thus making the asteroid appear smaller. This therefore shifts the hover point to a lower radius.

Simple approximations can be found as follows for the sunward and down-sun x-axis hover distances for a spacecraft equipped with a solar sail.

1) Sunward, for $a_{\max}$ other than very small, the sunward hover point is shifted so far from the asteroid that the gravitational attraction of Eros on the spacecraft becomes negligible. The term μ_{ast} in Eq. (7) can then be neglected, giving $3n^2|x|^3 - a_{\max}|x|^2 \approx 0$, or

$$|x_1| \approx a_{\max}/3n^2 \tag{23}$$

2) Down-sun, for $a_{\max}$ other than very small, the down-sun hover point is shifted so near to the asteroid that the gravitational attraction of the asteroid on the spacecraft becomes dominant. The term $3n^2x^3$ in Eq. (19) can then be neglected, giving $a_{\max}x^2 - \mu_{\text{ast}} \approx 0$, or

$$x_2 \approx \sqrt{\mu_{\text{ast}}/a_{\max}} \tag{24}$$

In addition to these two points on the x axis, more general hover points ($x \quad y \quad z$) will also exist for which $y \neq 0$ and/or $z \neq 0$. Any such point must satisfy the hover conditions of Eq. (16) as well as the magnitude condition $a_x^2 + a_y^2 + a_z^2 = a_{\text{tot}}^2$ of Eq. (15). The latter can therefore be written in terms of position as

$$A^2(r)x^2 + B^2(r)y^2 + C^2(r)z^2 = a_{\text{tot}}^2 \tag{25}$$

In addition, of course, the radius r that specifies $A(r)$, $B(r)$, and $C(r)$ is given as

$$x^2 + y^2 + z^2 = r^2 \tag{26}$$

These two conditions are analogous to the energy ellipsoid/momentum sphere approach to the solution of Euler's equations of rotational motion for a torque-free rigid body [12]. In the present problem, the position vector plays the role taken by the angular momentum vector in the rotational problem. In both cases, the solution(s) must lie on the intersection of an ellipsoid [defined in the asteroid problem by Eq. (25), with semi-axes $a_{\text{sail}}/A(r)$, $a_{\text{sail}}/B(r)$, and $a_{\text{sail}}/C(r)$] and a sphere [defined by Eq. (26), with radius r]. The difference is that in the current problem, the shape of the ellipsoid depends on the radius r, rather than being fixed by the moments of inertia of the body. In fact, the ellipsoid of Eq. (25) departs further from the spherical as r increases, because the terms involving n^2 in $A(r)$ and $C(r)$ become larger relative to μ_{ast}/r^3. This reflects the essential nonlinearity of the problem of locating hover points near an asteroid.

A question of practical interest is as follows: What is the closest point to the asteroid at which a solar sail can hover? As shown by Eqs. (17) and (18), a hover at a range of less than the libration point distance r_L [Eq. (19)] is certainly only possible on the antisun side of the asteroid. Equation (24) then defined the distance x_2 of the antisun hover point that lies on the x axis. However, can closer hover points be found by relaxing the constraints $y = z = 0$? To answer this question, consider any hover point ($x \quad y \quad z$) that is relatively close

to the asteroid. At this short range, the gravitational attraction of the asteroid will dominate over the heliocentric rotating frame effects in Eq. (16): that is,

$$A(r) \approx C(r) \approx B(r) = \mu_{\text{ast}}/r^3$$

consequently, $x \approx a_x(r^3/\mu_{\text{ast}})$. Likewise, the solar radiation acceleration vector must be approximately radial to counter the dominant (radial) asteroid attraction; this implies that $a_x/a_{\text{sail}} \approx x/r$. Comparing this with Eq. (15a) yields $\cos\alpha \approx x/r$, and thus $a_{\text{sail}} \approx a_{\max}(x/r)^2$. The acceleration component a_x can then be rewritten as $a_x \approx a_{\text{sail}}(x/r) \approx a_{\max}(x/r)^3$, which in turn implies that the x component of hover position satisfies

$$x \approx a_x(r^3/\mu_{\text{ast}}) \approx a_{\max}(x/r)^3(r^3/\mu_{\text{ast}}) = a_{\max}(x^3/\mu_{\text{ast}})$$

Hence, we must have that

$$x \approx \sqrt{\mu_{\text{ast}}/a_{\max}} = x_2 \tag{27}$$

the x-axis down-sun hover point defined by Eq. (24). We therefore expect hovering solutions to have x components near x_2.

An important variable for determining which hover points are of practical interest as locations from which to observe the asteroid is the *viewing angle*:

$$\gamma = \sin^{-1}(x/r) = \tan^{-1}(x/\sqrt{y^2+z^2}) \tag{28}$$

This angle quantifies how far down-sun of the terminator the spacecraft line of sight to the asteroid is located; if γ is relatively small, the hovering spacecraft will have something approaching half of the illuminated face of the asteroid in view.

A possible numerical method for computing all close-in (and thus necessarily down-sun from the center of the asteroid) hover points can be summarized as shown in Algorithm 1.

Numerical results will now be given for the illustrative case of heliostationary flight in the vicinity of a hypothetical spherical asteroid with the same radius, mass, and orbital semimajor axis as Eros. The asteroid has a heliocentric mean motion value of 1.13×10^{-7} rad/s and a sun–asteroid libration radius R_L of approximately 2266 km. Its mass is somewhat higher than that of a typical asteroid [4], making hovering flight rather challenging. Figure 3 plots the sunward hover distance for a solar sail-equipped spacecraft [given by Eq. (21)] as a function of its area-to-mass ratio A/m for values between 0 and 100 m^2/kg. For the fully unfurled ANTS value of 100 m^2/kg [1,2], the resulting distance is approximately 9.4×10^6 km, which is quite considerable and certainly not useful as a range from which to observe the asteroid. Figure 4 then plots the down-sun hover distance [from Eq. (22)] vs sail/spacecraft area-to-mass ratio, again for the range 0–100 m^2/kg. For the maximum ANTS A/m value, the resulting hover distance is 35.2 km; this is more potentially useful, although shadowing by the asteroid would likely prove to be a problem. Note that the errors between the approximate solutions given by Eqs. (23) and (24) and the true solutions from Eqs. (21) and (22) are quite modest. For instance, the down-sun approximation is accurate to within 1 km for all A/m values above 0.85 m^2/kg; this error is not distinguishable on the scale of Fig. 4.

Algorithm 1 Hover point calculation

For each x, $0 \le x \le r_L$.
  For each possible radius value r, $x \le r \le r_L$.
    Compute the quantities $A(r)$, $B(r)$, and $C(r)$.
    Hence, find $a_x = A(r)x$, and thus $\alpha = \cos^{-1}(\sqrt[3]{a_x/a_{\max}})$ and $a_{\text{tot}} = a_{\max}\cos^2\alpha$.
    Subtracting $B^2(r)$ times Eq. (26) from Eq. (25) gives an expression for z^2:

$$z^2 = [(a_{\text{sail}}^2 - a_x^2) - B^2(r)(r^2 - x^2)]/[C^2(r) - B^2(r)]$$

    Correspondingly, $y^2 = r^2 - x^2 - z^2$.
    If $y^2 \ge 0$ and $z^2 \ge 0$, the four points $(x \quad y \quad z)$, $(x \quad y \quad -z)$, $(x \quad -y \quad z)$, and $(x \quad -y \quad -z)$ are valid hover solutions. If not, no hover point exists for this x value.

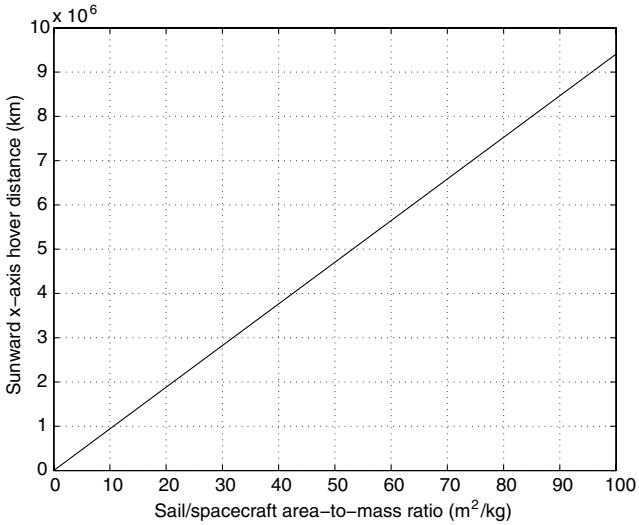

Fig. 3 Sunward x-axis hover-point distance vs A/m.

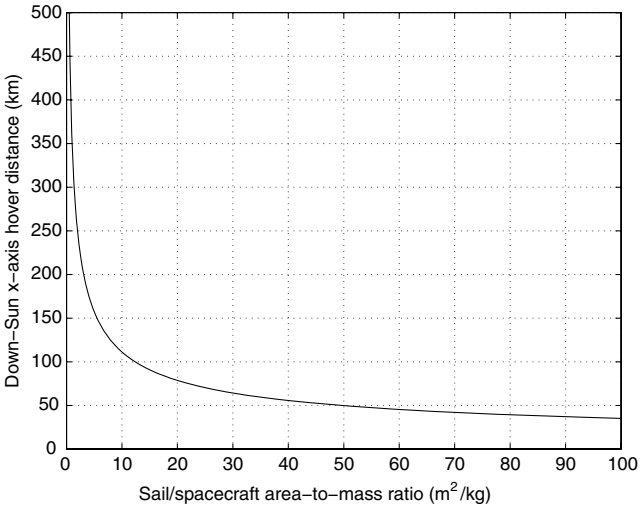

Fig. 4 Down-sun x-axis hover-point distance vs A/m.

Figure 5 next shows the sets of offaxis hover points obtained using the algorithm given previously for a sail/spacecraft area-to-mass ratio of 50 m^2/kg or with the ANTS sail half-furled. Each of the curves shows all possible y and z hover values for a specified value for x; the innermost curve corresponds to $x = 50$ km, and the successively larger curves correspond to x values of 70, 90, 110, 130, 150, and 170 km, respectively. Note that the smallest x for which a hover solution $(x \quad y \quad z)$ is found to exist using the numerical technique described previously is 49.77 km; this agrees well with the value of 49.75 km for x_2 for this A/m, which is given by Eq. (24).

Note that the curves in Fig. 5 are, to a first approximation, circular; this agrees with the previously observed fact that $A(r) \approx B(r) \approx C(r)$ for small r, thus rendering the ellipsoid of Eq. (25) approximately spherical. Consequently, little information is lost if the only hover points that are plotted are those that lie in the orbital plane of the asteroid (i.e., those for which $z = 0$). (From Eqs. (15) and (16), the sail clock angle ψ must be zero or π for any such hover point.) Figure 6 plots the locus of these points for x values up to 60 km for four different spacecraft area-to-mass ratios: 40 m^2/kg (solid curve), 50 m^2/kg (dotted curve), 60 m^2/kg (dashed-dotted curve), and the ANTS maximum of 100 m^2/kg (dashed curve). The figures also indicate the down-sun x-axis hover points x_2 for each value of A/m, as computed by Eq. (24). Very good agreement is again observed between these values (55.62, 49.75, 45.41, and 35.18 km for 40, 50,

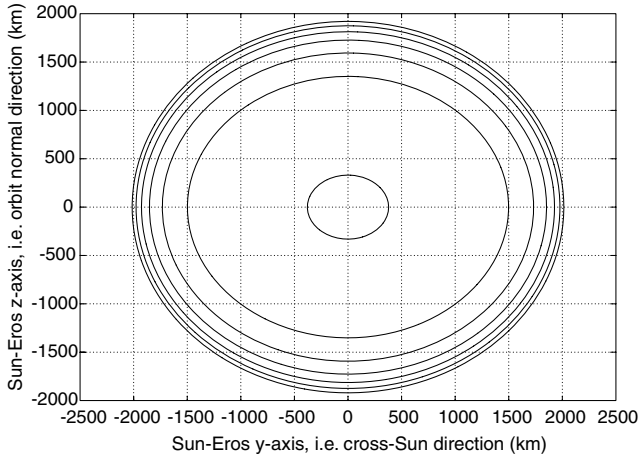

Fig. 5 Hover point contours for x from 50 to 170 km.

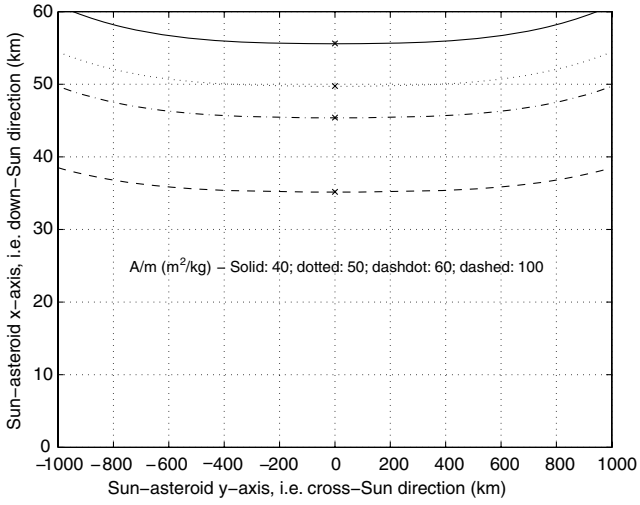

Fig. 6 In-plane hover-point curves vs A/m.

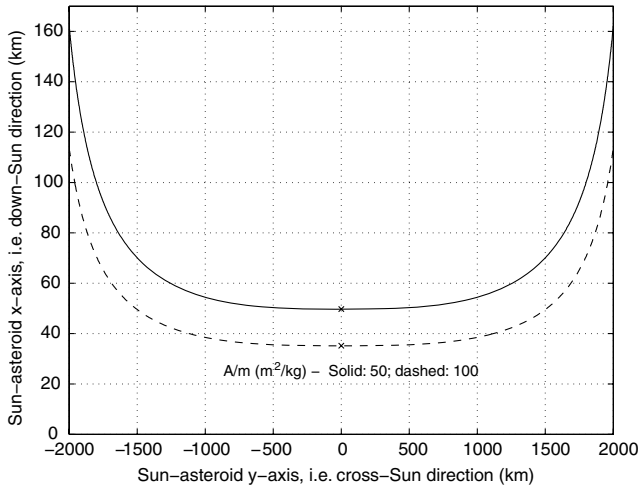

Fig. 7 Extended in-plane hover-point curve.

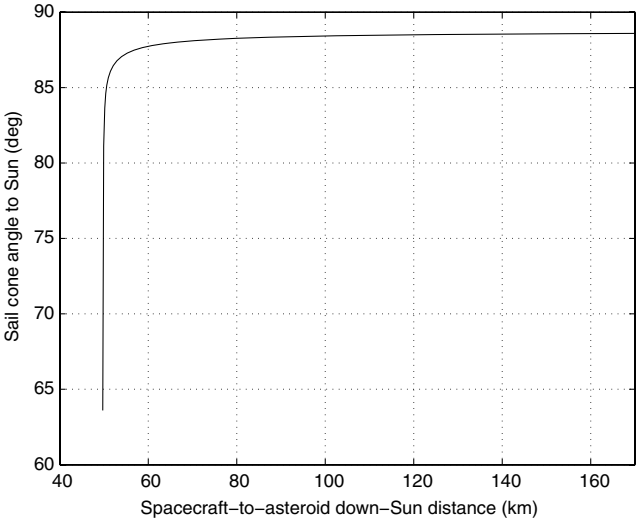

Fig. 8 In-plane hover sail cone angle.

60, and 100 m^2/kg, respectively) and the smallest x values for which the preceding algorithm returns valid hover solutions (55.65, 49.77, 45.44, and 35.21 km, respectively). In addition, the x coordinates of the hover solutions can be seen to vary only slowly in comparison with their y components in this region.

The curves of Fig. 6 should not be confused with the well-known *zero-velocity contours* of, for instance, [13–15]. The latter are contours of zero kinetic energy for no applied nongravitational force and provide boundaries that cannot be crossed by a body with given initial conditions. By contrast, the hover contours presented here are the sets of those points for which velocity and acceleration can be made zero by means of the solar radiation force. See [6] for a detailed discussion of the connections between the zero-velocity contours and hovering flight with a constant applied (propulsive) thrust vector.

Figure 7 shows the in-plane hover solution contour extended to a maximum x value of 170 km for area-to-mass ratios of 50 m^2/kg (solid curve) and 100 m^2/kg (dashed curve), and Fig. 8 plots the sail cone angle α corresponding to the 50 m^2/kg case. It can be seen that hover points corresponding to a range of relatively small x values can have fairly short ranges and low viewing angles down-sun of the terminator. Such positions may therefore prove to be useful as points from which to make close observations of a significant portion of the illuminated face of the asteroid. These side hover points (becoming regions for spacecraft such as ANTS with variable-area sails) compare favorably with the extremely-long-range hover [Eq. (21)] that could be achieved by a solar sail above the asteroid subsolar point. However, the large values for the sail angle α given in Fig. 8 should be recognized: to apply the required hovering force vector, the sail needs to be nearly edge-on to the sun. It is in this regime that real sail effects [3] such as diffuse reflection can lead to significant differences from the assumed ideal sail model. Consequently, a physical sail-equipped spacecraft may experience difficulties when attempting to carry out heliostationary flight above the example asteroid, even though the same sail is capable (see Figs. 1 and 2) of performing very rapid orbital changes about the same body.

Body-Fixed Hovering

Rather than maintaining a fixed position in the sun–asteroid (libration point) frame, as in the hovering problem, the spacecraft could instead be required to maintain a fixed position relative to a point on the surface of the rotating asteroid. This motion would allow prolonged observation of, for instance, a specific crater or other surface feature. To distinguish this from the heliostationary flight problem, this can be termed the *asterostationary flight* problem or, in the terminology of [5–8], *body-fixed hovering*. For a spacecraft devoid of a solar sail or other maneuvering capability, such flight is only possible at those points that lie above the asteroid equator at the *synchronous orbit radius* (or *resonance radius*, in the terminology of, for example, [7]):

$$r_{\text{sync}} = \sqrt[3]{\mu_{\text{ast}}/\omega_{\text{ast}}^2} \tag{29}$$

where ω_{ast} is the asteroid rotation rate. The addition of a thrusting capability (in particular, a solar sail here) will allow body-fixed hovering at more general locations; the question to be addressed here

is the extent to which the feasible region(s) will be enlarged for a given asteroid and sail A/m.

To analyze this problem, we first define a (near) nonrotating coordinate system, centered on the asteroid, with the $+z$ axis lying along the asteroid angular velocity vector (spin axis); the x and y axes ling in the asteroid equatorial plane, making up a right-handed triad; and the $+x$ axis directed away from the projected line to the sun. The unit vector directed from the sun to the asteroid is then given in this coordinate frame as

$$\hat{\mathbf{s}} = \begin{pmatrix} \cos\varphi \\ 0 \\ -\sin\varphi \end{pmatrix} \tag{30}$$

where the angle φ is the *solar latitude* (i.e., the perpendicular angle between the sun line and the equatorial plane of the asteroid).

The goal in the body-fixed hovering problem is to fly in a non-Keplerian orbit at a radius r above a point on the surface of the asteroid at latitude λ. The desired position of the spacecraft in this same coordinate system is therefore given as

$$\mathbf{r} = r\begin{pmatrix} \cos\lambda\cos\theta \\ \cos\lambda\sin\theta \\ \sin\lambda \end{pmatrix} \tag{31}$$

where θ is a longitude angle that reflects the rotation of the asteroid: $\theta(t) = \theta_o + \omega_{\text{ast}}t$, taking all values from 0 to 2π.

If we again assume for simplicity that the gravitational potential of the asteroid is spherically symmetric, the gravitational acceleration that it exerts on a spacecraft at this position is given as

$$\mathbf{a}_g = -\frac{\mu_{\text{ast}}}{r^3}\mathbf{r} = -\frac{\mu_{\text{ast}}}{r^2}\begin{pmatrix} \cos\lambda\cos\theta \\ \cos\lambda\sin\theta \\ \sin\lambda \end{pmatrix} \tag{32}$$

But the acceleration that is required to set up the desired spacecraft rotation about the asteroid spin axis at the asteroid rate is given as

$$\mathbf{a}_{\text{des}} = -r\omega_{\text{ast}}^2\begin{pmatrix} \cos\lambda\cos\theta \\ \cos\lambda\sin\theta \\ 0 \end{pmatrix} \tag{33}$$

Consequently, the acceleration that must be produced by the solar sail is

$$\mathbf{a}_{\text{sail}} = \mathbf{a}_{\text{des}} - \mathbf{a}_g = \begin{pmatrix} [(\mu_{\text{ast}}/r^2) - r\omega_{\text{ast}}^2]\cos\lambda\cos\theta \\ [(\mu_{\text{ast}}/r^2) - r\omega_{\text{ast}}^2]\cos\lambda\sin\theta \\ (\mu_{\text{ast}}/r^2)\sin\lambda \end{pmatrix} \tag{34}$$

Consider now the case in which no limits are imposed on the sail area-to mass ratio A/m. In this case, body-fixed hovering will be feasible if the desired sail acceleration $\mathbf{a}_{\text{sail}}$ remains down-sun as θ ranges between 0 and 2π. In other words, body-fixed hovering will be achievable for all spacecraft locations (described by the parameters r and λ) for which $\mathbf{a}_{\text{sail}} \cdot \hat{\mathbf{s}}$ remains positive for all longitudes θ. But, from Eqs. (30) and (34),

$$\mathbf{a}_{\text{sail}} \cdot \hat{\mathbf{s}} = -[(\mu_{\text{ast}}/r^2) - r\omega_{\text{ast}}^2]\cos\lambda\cos\theta\cos\varphi - (\mu_{\text{ast}}/r^2)\sin\lambda\sin\varphi \tag{35}$$

First, note that if we are to have $\mathbf{a}_{\text{sail}} \cdot \hat{\mathbf{s}} > 0$ for all θ, the second (constant) term in this expression must be positive, to overcome the alternating sign of $\cos\theta$ in the first term. Hence, we must have $\sin\lambda\sin\varphi < 0$, or (because $-\pi/2 \le \lambda$ and $\varphi \le \pi/2$) λ and φ must be of opposite signs. Thus, for instance, if the sun is below the asteroid equator, the spacecraft can only perform body-fixed hovering above points in the asteroid's northern hemisphere. (Note that this is not the same as saying that body-fixed hovering can only be performed above the shadowed hemisphere of the asteroid.)

Second, the critical longitude θ^* (if any) at which the sail becomes edge-on to the sun can be found from the switching condition $\mathbf{a}_{\text{sail}} \cdot \hat{\mathbf{s}} = 0$, giving from Eq. (35),

$$\cos\theta^* = -\frac{(\mu_{\text{ast}}/r^2)}{[(\mu_{\text{ast}}/r^2) - r\omega_{\text{ast}}^2]}\tan\lambda\tan\varphi = -\frac{1}{[1 - (\omega_{\text{ast}}/n)^2]}\tan\lambda\tan\varphi \tag{36}$$

where $n = \sqrt{\mu_{\text{ast}}/r^3}$ is the mean motion corresponding to a circular orbit about the asteroid at the spacecraft radius. For the given parameters φ, λ, and r (defining n), if the right-hand side of this equation has magnitude greater than unity, the switching condition $\mathbf{a}_{\text{sail}} \cdot \hat{\mathbf{s}} = 0$ is never encountered for any θ: body-fixed hovering is feasible (as long as λ and φ are of opposite signs). On the other hand, if the magnitude of the right-hand side of Eq. (36) is 1 or less, the desired sail acceleration will become up-sun for some longitude value(s); body-fixed hovering is therefore not feasible.

Analysis of Eq. (36) for the critical case $\cos\theta^* = \pm 1$ leads to the following ranges of spacecraft positions for which body-fixed hovering is feasible:

1) The feasible latitude range for given r and φ is $|\lambda^*| < |\lambda| < \pi/2$, where

$$\lambda^* = \arctan(\pm[1 - (\omega_{\text{ast}}/n)^2]\cot\varphi) \tag{37}$$

This describes a region around the asteroid pole that lies farther from the sun.

2) The range of feasible radii for given λ and φ is delimited by the critical condition (obtained using $(\omega_{\text{ast}}/n)^2 = r^3\omega_{\text{ast}}^2/\mu_{\text{ast}}$):

$$1 - r^{*3}\omega_{\text{ast}}^2/\mu_{\text{ast}} = -\text{sign}(\cos\theta^*)\tan\lambda\tan\varphi$$

or

$$r^{*3} = (\mu_{\text{ast}}/\omega_{\text{ast}}^2)[1 + \text{sign}(\cos\theta^*)\tan\lambda\tan\varphi] \tag{38}$$

Recalling that λ and φ must be of opposite signs, and thus $\tan\lambda\tan\varphi$ must be negative, the resulting radius solution range can be shown to be given as $r_1^* < r < r_2^*$, where

$$r_1^{*3} = \max\{0, (\mu_{\text{ast}}/\omega_{ast}^2)[1 + \tan\lambda\tan\varphi]\} \tag{39}$$

$$r_2^{*3} = (\mu_{\text{ast}}/\omega_{\text{ast}}^2)[1 - \tan\lambda\tan\varphi] \tag{40}$$

An interesting question is the effect of the solar latitude φ on these feasible ranges. It can be shown that if $\varphi \to \pi/2$ (the sun approaches one pole of the asteroid), the feasible region for body-fixed hovering for unlimited sail A/m becomes the entire space above the opposite hemisphere. By contrast, as $\varphi \to 0$ (the sun approaches the asteroid equatorial plane), the feasible region shrinks to a shell of radius r_{sync} above the antisun hemisphere, plus a tube surrounding the antisun polar axis. The solar latitude therefore plays a crucial role in this problem. (The asteroid Eros presents an interesting case: its rotation axis essentially lies in its orbital plane, and thus φ takes all possible values over the course of one Eros year.)

If the maximum sail area is finite, the requirement that $\mathbf{a}_{\text{sail}}$ must have a magnitude consistent with Eq. (1) further restricts the feasible body-fixed hovering locations. For large A/m, the resulting feasible region approaches those given by Eqs. (37), (39), and (40); for small A/m, it shrinks to a small equatorial torus near the synchronous orbit points, plus a region surrounding part of the antisun pole, starting at radial position

$$r_{\text{pole}}^2 = \frac{\mu_{\text{ast}}}{2\eta p(A/m)\sin^2\varphi} \tag{41}$$

Figure 9 illustrates the key role of the solar latitude in the body-fixed hovering problem. The asteroid considered (shown at the lower center of the figure) is spherical with a diameter of 1.0 km, density of 2.4×10^3 kg/m^3, and rotational period of 9.0 h (with spin axis aligned with the z axis), and it is in a 2.7 AU orbit; the spacecraft A/m is 100 m^2/kg (ANTS fully deployed). The figure shows (the set of upper curves with vertical line of symmetry) the feasible regions for solar latitudes of -30, -60, and -90 deg, as well as the corresponding regions that are shadowed from the sun by the asteroid

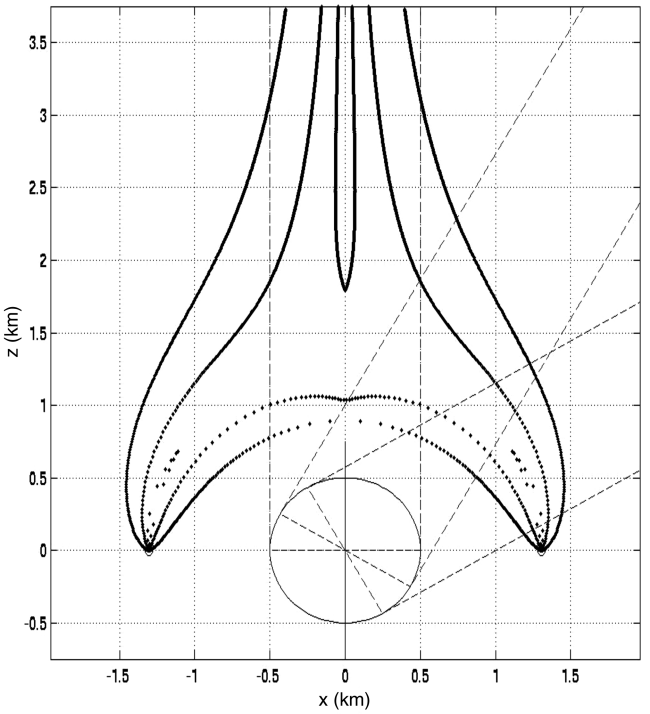

Fig. 9 Effect of solar latitude on body-fixed hovering performance.

(denoted by the angled dashed lines). It can be seen that the smallest feasible region, that corresponding to -30 deg, splits into a thin torus about the synchronous orbit points (at a radius of 1.31 km), together with a small tube about the pole. The feasible region corresponding to -60 deg is unified and somewhat larger, and that for -90 deg covers a significant region. The corresponding values for r_{pole} computed from Eq. (41) are 1.79, 1.03, and 0.894 km, respectively, which can be seen to agree with the plot.

Figure 10 then examines the role of A/m: the asteroid parameters are as described previously, except for the diameter, which is now 0.5 km. (The synchronous orbit radius for this asteroid is 0.653 km.) The zone that is shadowed from the sun by the asteroid is plotted as

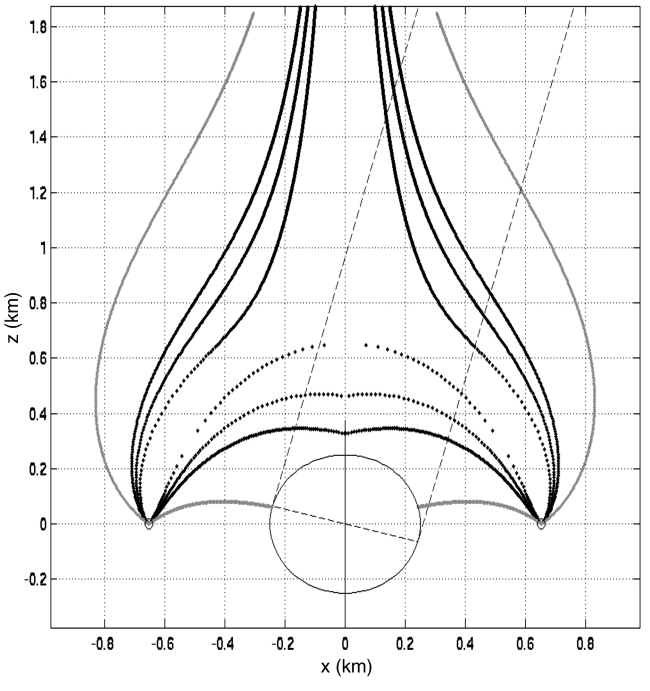

Fig. 10 Effect of sail area on body-fixed hovering performance.

before, but now for a fixed solar latitude of -75 deg. In addition, the feasible regions are plotted in black for three different values for A/m, representative of partially furled configurations for ANTS: 25, 50, and 100 m^2/kg. In addition, the feasible region for an unbounded maximum sail area is outlined in gray. The shrinking in the feasible curves that is produced by reducing the sail area is clear and is reflected by the increase in the corresponding r_{pole} values (0.327 km for 100 m^2/kg, 0.463 km for 50 m^2/kg, and 0.654 km for 25 m^2/kg).

Figures 9 and 10 taken together show that a spacecraft equipped with a solar sail with the ANTS maximum area-to-mass ratio can achieve a wide range of feasible body-fixed hovering positions for flight about an asteroid in this size range, typical of the main-belt population. The feasible body-fixed hovering locations are necessarily somewhat down-sun, from the nature of the solar force that acts on a solar sail; they can, however, still provide good views of a portion of the illuminated hemisphere of the asteroid, as well as of its terminator.

Conclusions

This paper has derived methods for quantifying the performance that can be achieved with a furlable solar sail, with area-to-mass ratio selectable up to some specified maximum value, when undertaking proximity operations at an asteroid. First, general non-Keplerian motion is examined in terms of the possible rates at which the sail can change the orbital elements of the spacecraft. Two types of hovering motion are then considered: one in which the spacecraft is required to maintain a fixed position in the rotating sun–asteroid frame and the other in which it is to stay fixed relative to the rotating asteroid surface. In both cases, the tight constraints on the sail force that are needed to produce the desired hovering motion, together with the down-sun nature of the solar force that acts on any solar sail and the correlation between solar force magnitude and direction, impose significant restrictions on the locations at which hovering flight can be achieved. For a spacecraft equipped with a sail of fixed area, these restrictions amount to the spacecraft being required to lie on two-dimensional surfaces relative to the asteroid. However, if a furlable sail is employed instead, these surfaces generalize to regions, thus providing significantly more freedom for the mission designer.

Acknowledgments

The authors wish to thank the Associate Editor and the anonymous reviewers for their valuable constructive comments.

References

[1] Curtis, S., Mica, J., Nuth, J., Marr, G., Rilee, M., and Bhat, M., "Autonomous Nano-Technology Swarm," International Astronautical Federation Paper 00-Q.5.08, Oct. 2000.

[2] Curtis, S. A., Rilee, M. L., Clark, P. E., and Marr, G. C., "Use of Swarm Intelligence in Spacecraft Constellations for the Resource Exploration of the Asteroid Belt," *Proceedings of the 3rd International Workshop on Satellite Constellations and Formation Flying*, Pisa, Italy, Feb. 2003.

[3] McInnes, C. R., *Solar Sailing: Technology, Dynamics and Mission Applications*, Springer–Verlag, New York,1999, pp. 11–13, 38–40, 47–53.

[4] Beatty, J. K., and Chaikin, A. (eds.), *The New Solar System*, 3rd ed., Cambridge Univ. Press, New York, 1990, pp. 231–240.

[5] Sawai, S., Scheeres, D. J., and Broschart, S., "Control of Hovering Spacecraft Using Altimetry," *Journal of Guidance, Control, and Dynamics*, Vol. 25, No. 4, 2002, pp. 786–795. doi:10.2514/2.4947

[6] Broschart, S. B., and Scheeres, D. J., "Boundedness of Spacecraft Hovering under Dead-Band Control in Time-Invariant Systems," *Journal of Guidance, Control, and Dynamics*, Vol. 30, No. 2, 2007, pp. 601–610. doi:10.2514/1.20179

[7] Broschart, S. B., and Scheeres, D. J., "Control of Hovering Spacecraft Near Small Bodies: Application to Asteroid 25143 Itokawa," *Journal of Guidance, Control, and Dynamics*, Vol. 28, No. 2, 2005, pp. 343–354. doi:10.2514/1.3890

[8] Morrow, E., Scheeres, D. J., and Lubin, D., "Solar Sail Orbit Operations at Asteroids," *Journal of Spacecraft and Rockets*, Vol. 38, No. 2, 2001, pp. 279–286. doi:10.2514/2.3682

[9] Scheeres, D. J., "Close Proximity and Landing Operations at Small Bodies," AIAA/AAS Astrodynamics Specialist Conference, AIAA Paper 96-3580, San Diego, CA, July 1996.

[10] Vallado, D. A., *Fundamentals of Astrodynamics and Applications*, 2nd ed., Microcosm/Kluwer, Dordrecht, The Netherlands, 2001 pp. 162–163, 374–379, 586–595.

[11] McInnes, C. R., MacDonald, M., Angelopolous, V., and Alexander, D., "GEOSAIL: Exploring the Geomagnetic Tail Using a Small Solar Sail," *Journal of Spacecraft and Rockets*, Vol. 38, July–Aug. 2001, pp. 622–629. doi:10.2514/2.3727

[12] Wertz, J. R. (ed.), *Spacecraft Attitude Determination and Control*, Kluwer Academic, London, 1978, pp. 499–501.

[13] Battin, R. H., *An Introduction to the Mathematics and Methods of Astrodynamics*, (rev. ed.), AIAA, Reston, VA, 1999, pp. 376–378.

[14] Lundberg, J., Szebehely, V., Nerem, R. S., and Beal, B., "Surfaces of Zero Velocity in the Restricted Problem of Three Bodies," *Celestial Mechanics*, Vol. 36, June 1985, pp. 191–205. doi:10.1007/BF01230651

[15] Moulton, F. R., *Introduction to Celestial Mechanics*, Macmillan, New York, 1914, pp. 281–294.

D. Spencer
Associate Editor